



## OPEN ACCESS

EDITED BY  
Hongbo Cong,  
University of Akron, United States

REVIEWED BY  
Qiao Yanxin,  
Jiangsu University of Science and  
Technology, China  
Da-Hai Xia,  
Tianjin University, China  
Michael F. Hurley,  
Boise State University, United States

\*CORRESPONDENCE  
Ziyan Zhu,  
zzhu46@uwo.ca

SPECIALTY SECTION  
This article was submitted to  
Environmental Degradation of Materials,  
a section of the journal  
Frontiers in Materials

RECEIVED 06 September 2022  
ACCEPTED 30 September 2022  
PUBLISHED 18 October 2022

CITATION  
Zhu Z, Ly M, Liu N, Noël JJ and  
Shoesmith DW (2022), The kinetics of  
hydrogen peroxide reduction on rare  
earth doped UO<sub>2</sub> and SIMFUEL.  
*Front. Mater.* 9:1038310.  
doi: 10.3389/fmats.2022.1038310

COPYRIGHT  
© 2022 Zhu, Ly, Liu, Noël and  
Shoesmith. This is an open-access  
article distributed under the terms of the  
[Creative Commons Attribution License  
\(CC BY\)](https://creativecommons.org/licenses/by/4.0/). The use, distribution or  
reproduction in other forums is  
permitted, provided the original  
author(s) and the copyright owner(s) are  
credited and that the original  
publication in this journal is cited, in  
accordance with accepted academic  
practice. No use, distribution or  
reproduction is permitted which does  
not comply with these terms.

# The kinetics of hydrogen peroxide reduction on rare earth doped UO<sub>2</sub> and SIMFUEL

Ziyan Zhu<sup>1\*</sup>, Malin Ly<sup>1</sup>, Nazhen Liu<sup>2</sup>, James J. Noël<sup>1,3</sup> and David W. Shoesmith<sup>1,3</sup>

<sup>1</sup>Department of Chemistry, The University of Western Ontario, London, ON, Canada, <sup>2</sup>Institute of Oceanology, Chinese Academy of Sciences, Qingdao, China, <sup>3</sup>Surface Science Western, The University of Western Ontario, London, ON, Canada

The electrochemical reduction of hydrogen peroxide has been studied in sodium chloride solutions containing various anions (bicarbonate/carbonate, sulphate) on Gd-UO<sub>2</sub>, Dy-UO<sub>2</sub> and a SIMFUEL (UO<sub>2</sub> doped to simulate spent nuclear fuel). The reaction was observed to proceed *via* the chemical oxidation of the surface to produce U<sup>V</sup> followed by its subsequent electrochemical reduction. The reaction was faster on the SIMFUEL surface due to the availability of the oxygen vacancies required to incorporate the O<sup>II</sup> ions necessary to maintain charge balance. Bicarbonate/carbonate, but not sulphate, was found to suppress peroxide reduction. This could be caused either by peroxide decomposition in solution or by the catalysis of peroxide reformation *via* the reaction of surface hydroxyl radicals with bicarbonate/carbonate to form carbonate radicals which subsequently decompose by reaction with water. The noble metal particles present in the SIMFUEL appear to play only a minor role in the reduction process.

## KEYWORDS

electrochemistry, SIMFUEL, hydrogen peroxide, UO<sub>2</sub>, rare earth dopants

## 1 Introduction

The prospects for the long-term containment of spent nuclear fuel in a deep geologic repository are very good (Kwong, 2011; Hall and Keech, 2017; Hall et al., 2021). However, it is judicious to assume some containers may fail before radiation fields have decayed to innocuous levels. It is also reasonable to assume that container failure leading to contact of the fuel with groundwater will not occur until β/γ radiation fields are negligible (a few hundred years) and only α-radiation fields remain significant (Badley and Shoesmith, 2022). Hence, a clear understanding of the influence of H<sub>2</sub>O<sub>2</sub>, the key oxidant produced by the α-radiolysis of H<sub>2</sub>O, on fuel corrosion and radionuclide release is important to elucidate the full mechanism of UO<sub>2</sub> corrosion. The influence of H<sub>2</sub>O<sub>2</sub> on UO<sub>2</sub> corrosion has been extensively studied and reviewed, with H<sub>2</sub>O<sub>2</sub> shown to both cause corrosion and undergo decomposition (Sunder et al., 2004; Nilsson and Jonsson, 2011; Eriksen et al., 2012; Lousada et al., 2013; Wu and Shoesmith, 2014; Liu et al., 2018; Zhu et al., 2020). This means it will be

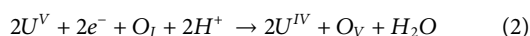
both anodically oxidized and cathodically reduced on the  $\text{UO}_2$  surface with its cathodic reduction being the key reaction supporting both dissolution and decomposition by disproportionation.

The kinetics of reduction processes on  $\text{UO}_2$  surfaces have been shown to be dependent on the chemical state of the surface, with electrochemical and X-ray photoelectron spectroscopy (XPS) studies demonstrating that reduction is blocked when an insulating  $\text{U}^{\text{VI}}$  oxide layer is present but proceeds rapidly on  $\text{U}^{\text{IV}}/\text{U}^{\text{V}}$  surfaces (Goldik et al., 2004; Goldik et al., 2005). Goldik et al. (2004), Goldik et al. (2005), Goldik et al. (2006a), Goldik et al. (2006b) interpreted the kinetics for  $\text{O}_2$  reduction using the mechanism proposed by Trunov and Presnov (1975a), Trunov and Presnov (1975b) on transition metal oxides and adopted by Hocking et al. (1991); Hocking et al. (1994) to explain the kinetics of  $\text{O}_2$  reduction on  $\text{UO}_2$ . According to this mechanism, electron transfer to adsorbed  $\text{O}_2$  molecules occurs at donor-acceptor relay (DAR) sites comprising  $\text{U}^{\text{IV}}$  and  $\text{U}^{\text{V}}$  in adjacent locations. The cathodic reduction of  $\text{O}_2$  is slow on  $\text{UO}_2$  but accelerated by oxidation of the surface to  $\text{U}_{1-2x}^{\text{IV}}\text{U}_{2x}^{\text{V}}\text{O}_{2+x}$  which provides the DAR sites to catalyze the electron relay process (Hocking et al., 1991; Hocking et al., 1994).

The kinetics of  $\text{H}_2\text{O}_2$  reduction on  $\text{UO}_2$  are considerably faster than those of  $\text{O}_2$ , since  $\text{H}_2\text{O}_2$  can chemically create, rather than rely on existing, DAR sites, a process accompanied by the incorporation of an oxygen interstitial ( $\text{O}_\text{I}$ ) into an oxygen vacancy ( $\text{O}_\text{V}$ ),



These sites are subsequently electrochemically destroyed by electron transfer with the  $\text{O}_\text{I}$  released (Hocking et al., 1991; Goldik et al., 2006b).



On SIMFUEL surfaces ( $\text{UO}_2$  doped with rare earths ( $\text{RE}^{\text{III}}$ ) and containing noble metal ( $\epsilon$ ) particles (Pd, Ru, Rh, Mo)), the kinetics of  $\text{O}_2$  reduction are catalyzed on the particle surfaces, leading to a notable increase in the overall reduction rate. However, electrochemical studies suggest only a minor influence of  $\epsilon$ -particles on  $\text{H}_2\text{O}_2$  reduction (Goldik et al., 2006a), since the rate on the DAR sites on the  $\text{UO}_2$  surface is already high. Goldik et al. (2005) demonstrated that the kinetics of  $\text{H}_2\text{O}_2$  reduction varied with the  $[\text{H}_2\text{O}_2]$  and the degree of oxidation of the  $\text{UO}_2$  surface. The formation of an insulating  $\text{U}^{\text{VI}}$  surface species suppressed the reduction by blocking DAR sites (Goldik et al., 2004).

The presence of  $\text{RE}^{\text{III}}$  dopants in  $\text{UO}_2$  has been shown to stabilize the  $\text{UO}_2$  matrix with charge balance maintained by the creation of  $\text{RE}^{\text{III}}-\text{O}_\text{V}$  and  $\text{U}^{\text{V}}$  sites (Razdan and Shoesmith, 2014; Liu et al., 2017a; Liu et al., 2017b). This study investigates the influence of  $\text{RE}^{\text{III}}$  doping on the kinetics of  $\text{H}_2\text{O}_2$  reduction using a combination of electrochemical techniques and Raman spectroscopy.

## 2 Experimental

### 2.1 Materials

The materials used in this study were a 3 at% SIMFUEL ( $\text{UO}_2$  doped with Sr, Y, Ce, Nd, La, Zr, Ba, Pd, Ru, Rh, and Mo to simulate in-reactor irradiation), 6.0 wt%  $\text{Gd}_2\text{O}_3$  in  $\text{UO}_2$  (Gd- $\text{UO}_2$ ) and 12.9 wt%  $\text{Dy}_2\text{O}_3$  in  $\text{UO}_2$  (Dy- $\text{UO}_2$ ). The SIMFUEL and Dy- $\text{UO}_2$  were fabricated by Canadian Nuclear Laboratories (Chalk River, Ontario, Canada) and the Gd- $\text{UO}_2$  supplied by Cameco (Port Hope, Ontario, Canada). Rotating disc electrodes, approximately 2–3 mm thick and 12 mm in diameter, were cut from pellets and fabricated into electrodes using our previously described procedures (Santos et al., 2004). The resistivity values of the materials were: Gd- $\text{UO}_2$  (50  $\Omega$  cm), Dy- $\text{UO}_2$  (55  $\Omega$  cm) and SIMFUEL (82  $\Omega$  cm).

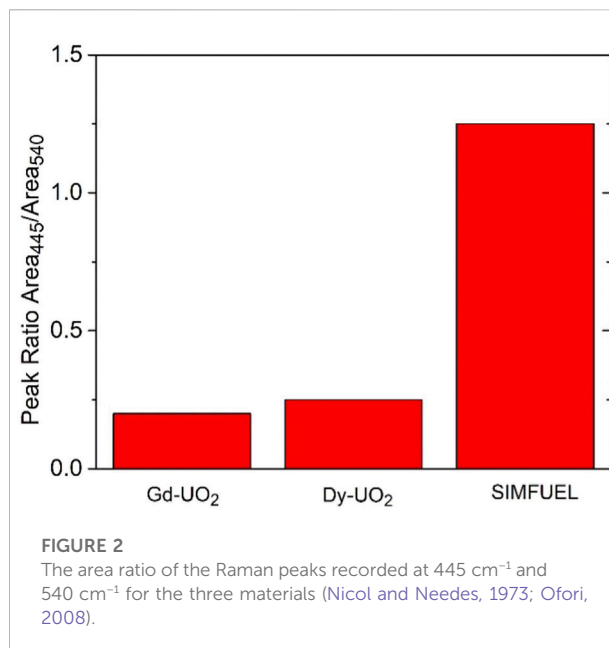
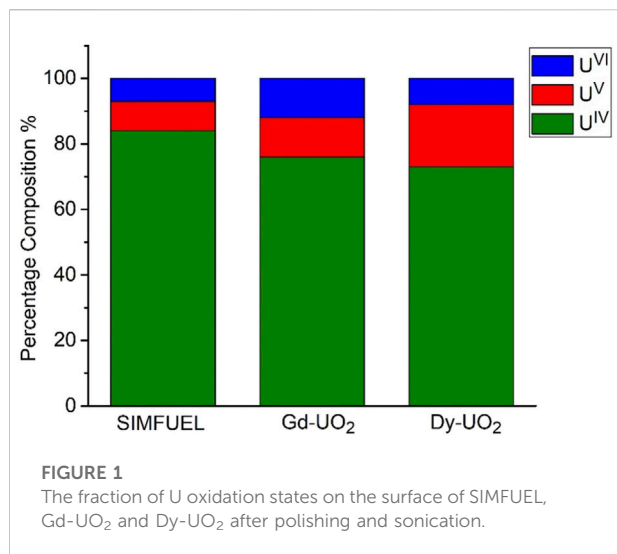
### 2.2 Electrochemical cell and procedures

A three compartment electrochemical cell was used in all experiments. A saturated calomel electrode (SCE) was used as the reference electrode, with a Pt mesh counter electrode spot welded to a Pt wire. The cell was placed inside a Faraday cage to prevent interference from external noise. Prior to each experiment, electrodes were wet-polished with 1200 SiC paper, rinsed with Type I  $\text{H}_2\text{O}$  and cathodically cleaned at a potential (E) of  $-1.2$  V (vs. SCE) for 2 min to reduce any air-formed oxide film.

A Solartron model 1287 potentiostat was used to apply potentials and record current responses. A potential scan rate of  $10$  mV  $\text{s}^{-1}$  was used in cyclic voltametric (CV) experiments with the current interrupt procedure adopted to compensate for electrode resistance (Britz and Brocke, 1975). Corrware (Scribner Associates) software was used to control instrumentation and analyze data. The rotation rate of the working electrode (WE) was controlled using an analytical model ASR rotator from Pine Instruments.

### 2.3 Solutions

All solutions were prepared with Type I  $\text{H}_2\text{O}$  with a resistivity of  $18.2$  M $\Omega$  cm, purified using a Millipore Milli-Q ion exchange column. Experiments were conducted at room temperature in solutions sparged with Ar [ultra high purity (Praxair)] for at least 30 min prior to each experiment, with sparging continued throughout each experiment. Experiments were performed in a  $0.1$  mol.L $^{-1}$  NaCl solution, with the final pH adjusted to 9.7 using NaOH solution. When required,  $\text{Na}_2\text{CO}_3$ ,  $\text{Na}_2\text{SO}_4$  and  $\text{H}_2\text{O}_2$  were added at the desired concentrations. All chemicals were reagent grade and purchased from Fisher Scientific.



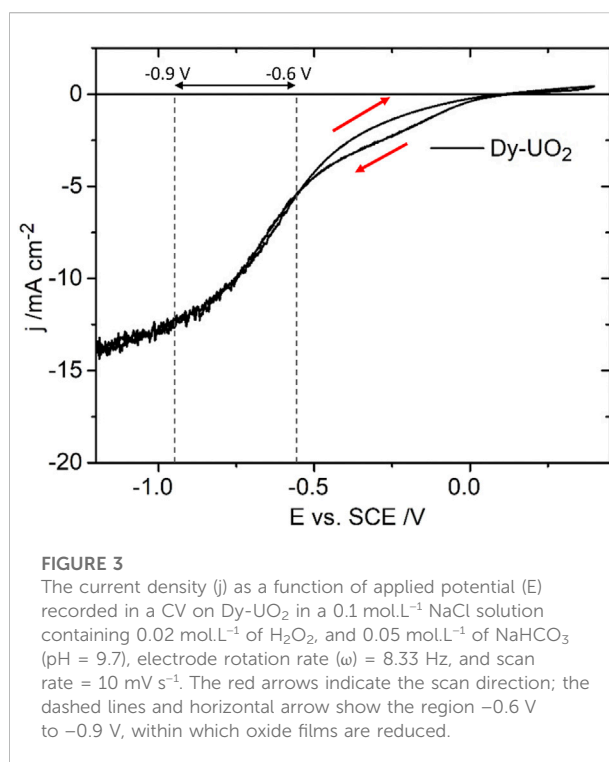
## 2.4 Analytical procedures

X-ray photoelectron spectroscopy (XPS) was performed using a Kratos Axis NOVA spectrometer with a monochromatic Al K<sub>α</sub> X-ray source (1486.6 eV). The instrument work function was calibrated to give a binding energy of 83.96 eV for the 4f<sub>7/2</sub> line for metallic Au, and the spectrometer dispersion was adjusted to give a binding energy (BE) of 932.62 eV for the 2p<sub>3/2</sub> line of metallic Cu. Survey scans were recorded over the energy range 0–1100 eV on an analysis area of 300 × 700 μm<sup>2</sup> with a pass energy of 160 eV. High resolution spectra were recorded at a pass energy of 20 eV with a step size of 0.05 eV. The C 1s peak at 285.0 eV was used as a standard, when required, to correct for surface charging. Spectra were analyzed using CasaXPS software (version 2.3.14). The fractions of U<sup>IV</sup>/U<sup>V</sup>/U<sup>VI</sup> in the electrode surfaces were obtained by deconvolution of the high resolution XPS spectra using curve fitting procedures and BEs described elsewhere (Ilton et al., 2007; Schindler et al., 2009; Razdan et al., 2012).

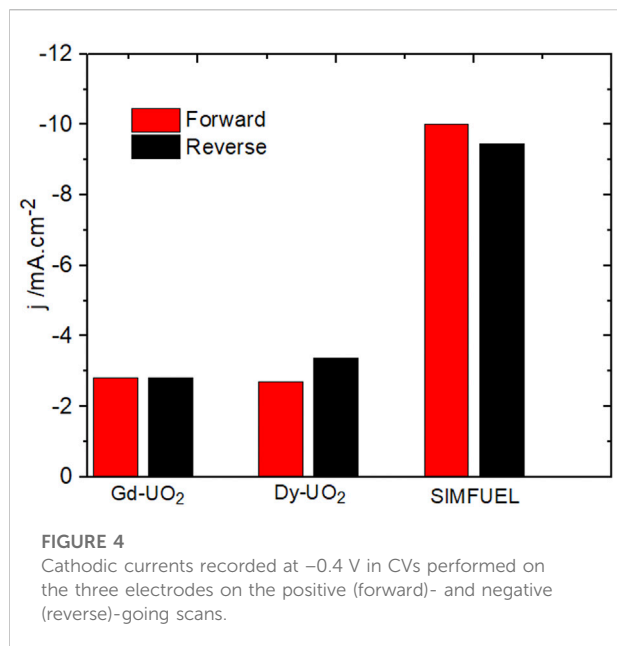
Surface characterization of the electrodes using scanning electron microscopy, energy dispersive X-ray spectroscopy, X-ray diffraction and Raman spectroscopy have been published previously (He et al., 2007; He et al., 2012; Razdan et al., 2014; Razdan and Shoosmith, 2014). These analyses demonstrate that the RE<sup>III</sup> dopants were uniformly distributed in the UO<sub>2</sub> matrix, not present as separate phases, with the noble metal (ε) particles predominantly, but not exclusively, located on grain boundaries (Zhu et al., 2019).

## 3 Results

Figure 1 shows the fractions of U<sup>IV</sup>/U<sup>V</sup>/U<sup>VI</sup>, obtained from XPS analyses, in the surfaces of the three electrodes. As expected,



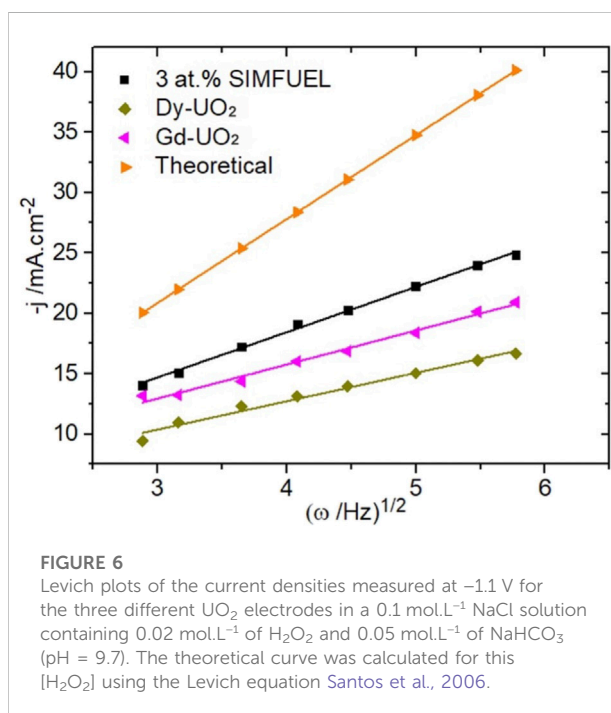
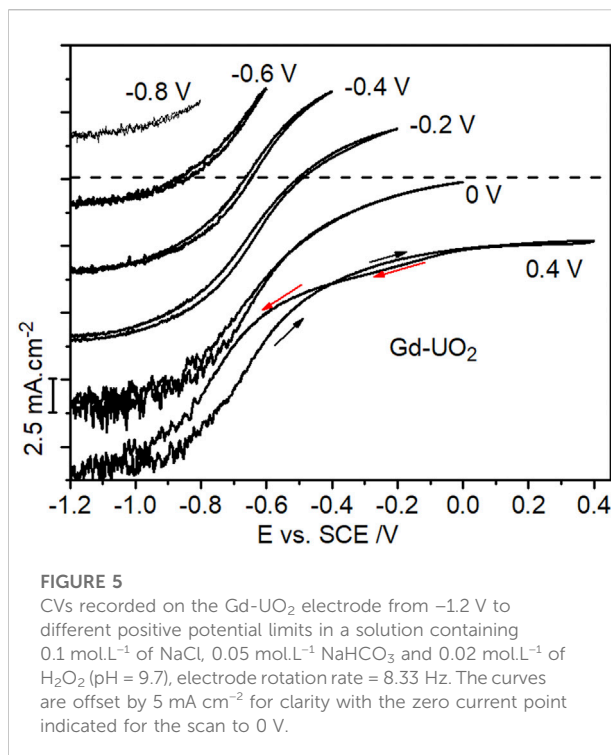
the U<sup>V</sup> content increases with the extent of RE<sup>III</sup> doping from the lightly doped SIMFUEL to the heavily doped Dy-UO<sub>2</sub>. The small fractions of U<sup>VI</sup> present on all surfaces can be attributed to the presence of a thin air-formed layer since the electrodes were not subjected to cathodic reduction prior to recording the spectra. While XPS gives an indication of surface composition, Raman



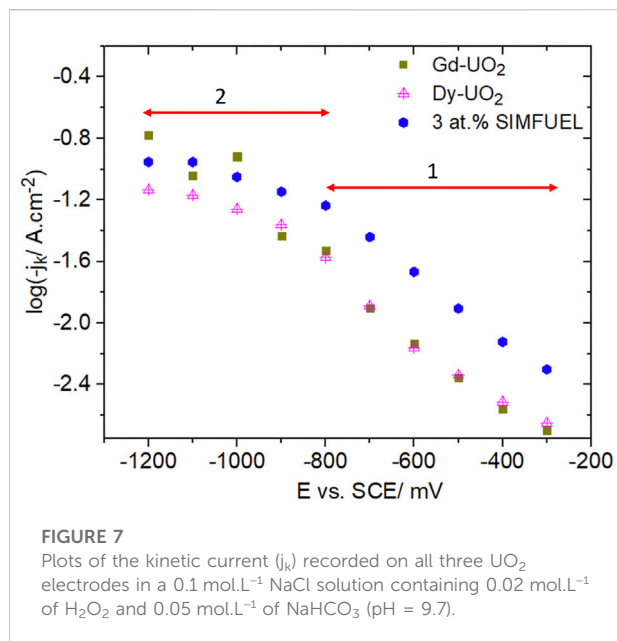
spectroscopy is a better indicator of the properties of the oxide matrix. Figure 2 shows the area ratio between the  $T_{2g}$  Raman peak ( $445\text{ cm}^{-1}$ ) and the peak at  $540\text{ cm}^{-1}$  calculated from the Raman spectroscopy measurements of Razdan and Shoemith (2014). Since the  $T_{2g}$  peak is attributed to the fundamental U-O stretch, it is characteristic of the undisturbed  $\text{UO}_2$  fluorite lattice, while the peak at  $540\text{ cm}^{-1}$  is a measure of the  $\text{RE}^{\text{III}}\text{-O}_V$  clustering, a process which would be expected to limit the availability of the  $\text{O}_V$  required for reaction 1 (He and Shoemith, 2010).

Figure 3 shows a CV recorded on the Dy- $\text{UO}_2$  electrode over the potential range from  $-1.2$  V to  $0.4$  V (vs. SCE) in a NaCl solution containing both  $\text{H}_2\text{O}_2$  and  $\text{HCO}_3^-/\text{CO}_3^{2-}$ . On the positive-going scan, a minor oxidation process is observed for  $E \geq 0.1$  V (vs. SCE), leading to a slight enhancement of the cathodic current on the negative-going scan in the E range from  $0$  V to  $-0.5$  V (vs. SCE). In the absence of  $\text{H}_2\text{O}_2$ , a voltametric scan over the same potential range yielded a similar minor oxidation on the positive-going scan, leading to a shallow reduction peak between  $-0.6$  V and  $-0.9$  V (the potential range indicated by the horizontal arrow in Figure 3). Similar differences (not shown) were observed between the positive- and negative-going scans on the Gd- $\text{UO}_2$  and SIMFUEL electrodes, with the currents on both the positive- and negative-going scans being significantly higher for the SIMFUEL, as shown for  $E = -0.4$  V (vs. SCE) in Figure 4. Since the SIMFUEL contains  $\epsilon$ -particles, there is a possibility they could act as catalytic locations for  $\text{H}_2\text{O}_2$  reduction. However, a previous study on a series of SIMFUELS suggested that, while this was the case, the effect was small (Goldik et al., 2006a).

Slightly enhanced currents on the negative-going scan recorded in  $\text{H}_2\text{O}_2$ -containing solutions have tentatively been



assigned to the reduction of anodically-formed peroxycarbonate species ( $\text{U}^{\text{V}}\text{O}_2(\text{HCO}_3)(\text{H}_2\text{O}_2)$ ), which appear to catalyze  $\text{H}_2\text{O}_2$  reduction (Goldik et al., 2006b), and possibly



also to the reduction of  $\text{U}^{\text{VI}}$  peroxycarbonate species ( $\text{U}^{\text{VI}}\text{O}_2(\text{O}_2)_x(\text{CO}_3)_y^{2-2x-2y}$ ) which would be expected at the  $[\text{H}_2\text{O}_2]$  and  $[\text{CO}_3]_{\text{tot}}$  ( $[\text{CO}_3]_{\text{tot}} = [\text{HCO}_3^-] + [\text{CO}_3^{2-}]$ ) involved in this study (Zhu et al., 2019). On occasion, currents on the negative-going scan were lower than those recorded on the positive-going scan, a feature attributable to the need to reduce anodically formed insulating  $\text{U}^{\text{VI}}$  layers ( $\text{U}^{\text{VI}}\text{O}_3 \cdot 2\text{H}_2\text{O}/\text{UO}_2\text{CO}_3/\text{U}^{\text{VI}}\text{O}_4 \cdot 4\text{H}_2\text{O}$ ) (Zhu et al., 2019) in the potential region indicated by the horizontal arrow in Figure 3. Figure 5 shows CVs recorded on the Gd- $\text{UO}_2$  electrode in voltametric scans from  $E = -1.2 \text{ V}$  (vs. SCE) to various more positive potential limits, showing that these anodic complications can be minimized if this limit is restricted to  $< 0 \text{ V}$  (vs. SCE). Similar results (not shown) were observed on the other two materials.

Figure 6 shows  $\text{H}_2\text{O}_2$  reduction current densities, obtained from CVs, recorded as a function of electrode rotation rate ( $\omega$ ) at  $E = -1.1 \text{ V}$ , a potential in the apparently transport-controlled region ( $E \leq -1.0 \text{ V}$  (vs. SCE), Figure 5). Also shown is the diffusion-limited current calculated using the Levich equation (Santos et al., 2006) with a diffusion coefficient ( $D$ ) for  $\text{H}_2\text{O}_2 = 1.32 \times 10^{-5} \text{ cm}^2 \text{ s}^{-1}$  Trunov and Presnov (1975a) and a kinematic viscosity for the electrolyte of  $1.013 \times 10^{-2} \text{ cm}^2 \text{ s}^{-1}$  (Lide, 2005). While the currents are all linearly dependent on  $\omega^{1/2}$ , as expected according to the Levich relationship, they are lower than the calculated diffusion-limited current, demonstrating that total diffusion control was unattainable on all three materials. Also noteworthy are the relative values of the currents, which decrease with the level of  $\text{RE}^{\text{III}}$ -doping (SIMFUEL  $>$  Gd- $\text{UO}_2$   $>$  Dy- $\text{UO}_2$ ).

Currents for  $\text{H}_2\text{O}_2$  reduction were measured as a function of potential and electrode rotation rate ( $\omega$ ). Using the Koutecky-Levich approach (Bard and Faulkner, 2000) and assuming a

reaction order of 1 (the efficacy of choosing such a value is discussed in reference 13), currents were corrected for the influence of transport and the change in pH due to  $\text{OH}^-$  production at the electrode surface to yield the kinetic currents plotted in the Tafel format in Figure 7. Two distinct regions of linear behaviour were observed, suggesting a change in the rate-determining reaction from the electrochemical reduction of the  $\text{U}^{\text{V}}$  intermediate in region 1 (Figure 7) (reaction 2) to the chemical formation of  $\text{U}^{\text{V}}$  in potential region 2 (Figure 7) (reaction 1). In region 1 the currents observed for Dy- $\text{UO}_2$  and Gd- $\text{UO}_2$  are effectively the same, while the currents for the SIMFUEL are significantly higher. The order of reactivity of the electrodes in region 1 (SIMFUEL  $>$  Gd- $\text{UO}_2 \sim$  Dy- $\text{UO}_2$ ) is the same as observed for their susceptibility to anodic dissolution at more positive potentials (Liu et al., 2017a). The similar Tafel slopes indicate that the mechanism of reduction is the same on all three materials. The transition between regions 1 and 2 was observed for all three materials and occurred over the potential range within which surface oxides become unstable and electrochemically reduced (as indicated by the horizontal arrow in Figure 3).

Reaction orders in region 1 (Figure 7), measured over the range  $0.01 \leq [\text{H}_2\text{O}_2] \leq 0.2 \text{ mol/L}^{-1}$  in the absence of  $\text{HCO}_3^-/\text{CO}_3^{2-}$  to avoid the complications discussed below, yielded values in the range 0.43–0.7 for the three materials. Attempts to measure reaction orders in region 2 were complicated by erratic currents attributable to the use of the current interrupt procedure, but yielded values in the range 1–1.5.

Figure 8 shows kinetic currents recorded for all three electrodes for two  $[\text{CO}_3]_{\text{tot}}$  (three for Dy- $\text{UO}_2$ ) showing that an increase in  $[\text{CO}_3]_{\text{tot}}$  caused both a decrease in current and an increase in Tafel slope (as indicated in the figures) for all three materials. For Gd- $\text{UO}_2$  and Dy- $\text{UO}_2$ , the Tafel slopes were effectively the same and increased slightly as  $[\text{CO}_3]_{\text{tot}}$  was increased. For both electrodes, but especially the Dy- $\text{UO}_2$ , the influence of  $[\text{CO}_3]_{\text{tot}}$  is minor at less negative potentials and increases as the potential is made more negative, indicating that when the electrochemical reaction 2 is slow compared to the chemical reaction 1,  $\text{HCO}_3^-/\text{CO}_3^{2-}$  exerts only a minor influence on the overall reaction kinetics. For the SIMFUEL, the Tafel slopes were significantly higher, especially at the lower concentration. The transition from potential region 1 ( $E \geq -0.9 \text{ V}$ ) to potential region 2 ( $E \leq -0.9 \text{ V}$ ) was clear for the SIMFUEL and Dy- $\text{UO}_2$  electrodes but only poorly defined for the Gd- $\text{UO}_2$  electrode. The inclusion of data for a third higher  $[\text{CO}_3]_{\text{tot}}$  on Dy- $\text{UO}_2$  confirmed that the influence of  $\text{HCO}_3^-/\text{CO}_3^{2-}$  was most marked in region 2.

Experiments in solutions containing  $\text{SO}_4^{2-}$  (not shown) rather than  $\text{HCO}_3^-/\text{CO}_3^{2-}$  showed no significant effect of this anion on  $\text{H}_2\text{O}_2$  reduction currents, confirming that the suppression of the  $\text{H}_2\text{O}_2$  reduction current was specific to  $\text{HCO}_3^-/\text{CO}_3^{2-}$ . This absence of an influence is not surprising since, unlike  $\text{HCO}_3^-/\text{CO}_3^{2-}$ ,  $\text{SO}_4^{2-}$  is not a strong complexant for

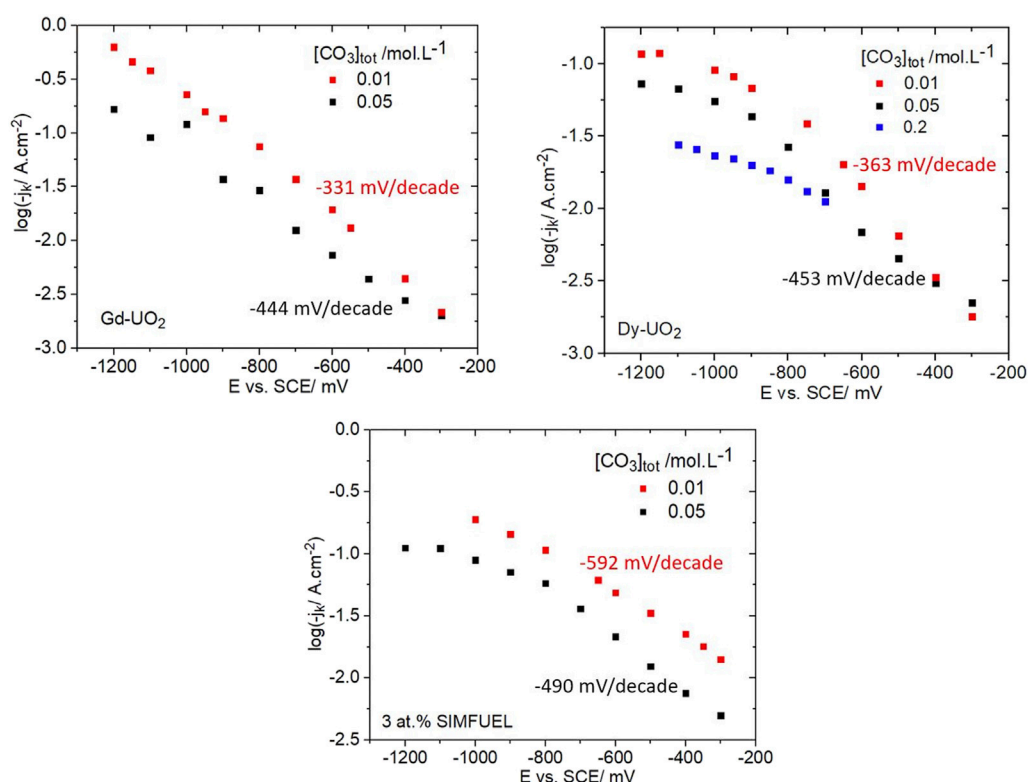


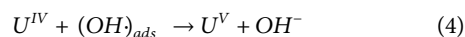
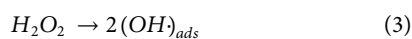
**FIGURE 8**

Plots of kinetic currents ( $j_k$ ) as a function of potential recorded on all three electrodes in a 0.1 mol.L<sup>-1</sup> NaCl solution containing 0.02 mol.L<sup>-1</sup> of H<sub>2</sub>O<sub>2</sub> (pH = 9.7) and two different [CO<sub>3</sub>]<sub>tot</sub> (three for Dy-UO<sub>2</sub>). The Tafel slopes indicated on the plots were calculated over the potential region from -0.3 V to -0.9 V.

soluble U species (Grenthe et al., 1992) and its influence on the electrochemistry of UO<sub>2</sub> has been shown to be limited to acidic solutions (Nicol and Neeves, 1973; Ofori, 2008).

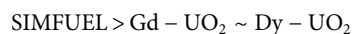
## 4 Discussion

Previously, we adopted the kinetic analysis developed for the reduction of H<sub>2</sub>O<sub>2</sub> on Cu (Vazquez et al., 1994; Ceré et al., 1999) to interpret the kinetics of its reduction on UO<sub>2</sub> (Goldik et al., 2006a). According to this analysis, the transition from a potential-dependent current at low cathodic overpotentials to a chemically-controlled current at high overpotentials can be attributed to the reaction scheme (1) and (2), involving chemical oxidation of the UO<sub>2</sub> surface to produce a U<sup>V</sup> intermediate, followed by its electrochemical reduction. The formation of U<sup>V</sup> is known to proceed *via* the initial formation of surface OH<sup>•</sup> radicals (Barreiro Fidalgo et al., 2018; Maier et al., 2020),



The formation of a U<sup>V</sup> surface state is also the first step in the anodic oxidation/dissolution of UO<sub>2</sub>, a reaction also involving the incorporation of O<sup>II</sup> into interstitial oxygen vacancy (O<sub>V</sub>) sites in the UO<sub>2</sub> matrix to produce a thin U<sub>1-2x}</sub><sup>IV</sup>U<sub>2x}</sub><sup>V</sup>O<sub>2+x</sub> surface layer (Goldik et al., 2004).

The involvement of O<sub>V</sub>s can also explain the order of H<sub>2</sub>O<sub>2</sub> reduction currents as demonstrated by Raman spectroscopy, Figure 2. Using the peak ratio as a measure of O<sub>V</sub> content, it is clear that their availability, and hence ability to support reaction 1, is in the order observed for H<sub>2</sub>O<sub>2</sub> reduction currents,



The similarity in reduction currents for Gd-UO<sub>2</sub> and Dy-UO<sub>2</sub>, despite the major differences in doping level, suggest that there may be a limit to the impact of RE<sup>III</sup> doping on the kinetics of H<sub>2</sub>O<sub>2</sub> reduction. An identical similarity was observed in their resistance to anodic dissolution (Liu et al., 2017b). The ability of UO<sub>2</sub> to function catalytically in this manner is similar to the well-recognized behaviour of CeO<sub>2</sub>, which also possesses a fluorite lattice containing O<sub>V</sub> and can be readily oxidized and reduced between Ce<sup>III</sup> and Ce<sup>IV</sup>. Both oxides possess the ability to incorporate and release O as indicated in reactions 1 and 2.

According to our previous studies (Goldik et al., 2005; Goldik et al., 2006a; Goldik et al., 2006b), the kinetic balance between reactions 1 and 2 determines both the Tafel slope and the reaction order with respect to  $H_2O_2$ , both of which are defined by the rate constants for these reactions (Vazquez et al., 1994; Ceré et al., 1999). The Tafel slope for reaction 2 is given by

$$\frac{d \log(-j_k)}{dE} = \frac{-\alpha_c F}{2.303RT} \left( \frac{X}{1-X} \right) \quad (5)$$

and the reaction order (m) by

$$m = \frac{1}{1+X} \quad (6)$$

with

$$X = \frac{k_c [H_2O_2]}{k_e} \quad (7)$$

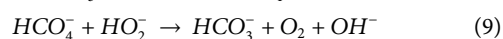
and  $k_c$  and  $k_e$  are the rate constants for reactions 1 and 2, respectively.

Based on these relationships, the large Tafel slopes and fractional reaction orders can be explained in terms of the relative rates of these two reactions. If the rate of reaction 1, the formation of the intermediate  $U^V$  state, was slow ( $k_c [H_2O_2] \ll k_e$ ), the overall reaction would be chemically controlled:  $X$  would become small, the reaction order (m) approach 1, and the Tafel slope become very large. If the rate of reaction 2, the electrochemical reduction of the  $U^V$  intermediate, was slow ( $k_c [H_2O_2] \gg k_e$ ), the overall reaction would be electrochemically controlled and  $X$  would tend to  $\infty$ ,  $m$  to 0, and the Tafel slope would approach the value of 120 mV/decade, as expected for a one-electron-transfer-controlled process.

The plots in Figure 7 are consistent with such an analysis. In region 1, the large Tafel slopes and fractional reaction orders are consistent with an overall reaction under mixed chemical/electrochemical control. All three materials exhibit similar values, with the only significant difference being the higher currents measured on the SIMFUEL, attributed (above) to the higher availability of  $O_V$ . In region 2, the switch to an almost potential-independent current and a reaction order in the region of 1 confirms that the overall reaction becomes chemically controlled at large negative potentials, when the electrochemical reaction would be rapid. The order of the current values changes, with that for the heavily doped Dy- $UO_2$  being less than the approximately equal values observed for Gd- $UO_2$  and SIMFUEL.

The absence of any influence of  $SO_4^{2-}$ , but a clear influence of  $HCO_3^-/CO_3^{2-}$ , on the  $H_2O_2$  reduction current indicates a direct involvement of the latter anion in the surface reduction process. A possibility is that the suppressed current on all three materials can be explained by the well documented ability of  $HCO_3^-/CO_3^{2-}$  to form

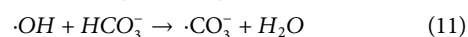
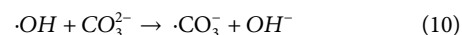
peroxycarbonates which catalyze  $H_2O_2$  decomposition in slightly alkaline solutions (Richardson et al., 2000)



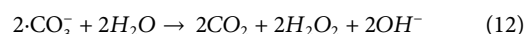
$HCO_4^-$  has been shown to be a kinetically more rapid oxidant than  $H_2O_2$  for various species (Richardson et al., 2000; Regino and Richardson, 2007), and could be so for  $UO_2$ , providing only minor consumption by decomposition on the time scale of our experiments. This would lead to an increase in the rate of reaction 1 and the overall reaction, a possible extension of region 1 to more negative potentials, and a decrease in the Tafel slope. The observation that Tafel slopes increase when the  $[CO_3]_{tot}$  is increased does not support this argument.

Since  $HCO_3^-/CO_3^{2-}$  is a strong complexant for oxidized states of U, both as surface species ( $U^V/U^{VI}$ ) (Keech et al., 2011) and as soluble species ( $U^{VI}O_2(CO_3)_x^{(2-2x)}$ ) (Mühr-Ebert et al., 2019; Grenthe and Gaona, 2020), it would be expected to accelerate the formation of  $U^V$  via reaction 1 and to stabilize it against subsequent electrochemical reduction by reaction 2. Such a process could lead to a suppression of the overall current, as observed, but not to an increased Tafel slope indicative of a slower chemical reaction relative to the rate of the electrochemical reaction.

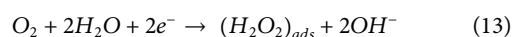
Since the reaction of  $H_2O_2$  proceeds through radical surface intermediates (reactions 3 and 4) and  $HCO_3^-/CO_3^{2-}$  has been shown to form radical species via reaction with radiolytically-produced  $\bullet OH$  (Haygarth et al., 2010),



it is likely that such carbonate radicals are formed on the  $UO_2$  surface and recombine to reform  $H_2O_2$ ,



with  $CO_2$  rapidly hydrolyzing to  $HCO_3^-$  at the pH employed in our study. Alternative pathways for this radical decay process have been demonstrated in radiolytic studies (Richardson et al., 2000; Barreiro Fidalgo et al., 2018; Maier et al., 2020). While speculative, some support for such a reforming of  $H_2O_2$  is provided in studies of the electrochemical reduction of  $O_2$  on  $UO_2$  (Nicol and Needes, 1973; Ofori, 2008), a reaction which can proceed via the formation of  $H_2O_2$  as an intermediate:



In the absence of  $HCO_3^-/CO_3^{2-}$ , this reaction proceeds efficiently with the release to solution of only minimal amounts of  $H_2O_2$ . In the presence of  $HCO_3^-/CO_3^{2-}$  measurable amounts of  $H_2O_2$  are released to solution, consistent with its partial stabilization in the presence of these anions.

The influence of  $[\text{CO}_3]_{\text{tot}}$  on  $\text{H}_2\text{O}_2$  reduction on the SIMFUEL is somewhat different from that observed on the other two materials, especially at low negative potentials in region 1. According to the reaction scheme proposed, this would suggest a very marked influence of  $\text{HCO}_3^-/\text{CO}_3^{2-}$  in reducing the rate of reaction 2 relative to reaction 1 by stabilizing the chemically formed  $\text{U}^{\text{V}}$  state. However, an increased Tafel slope, as observed (Figure 7), suggests the opposite. Previous studies on a series of SIMFUELS (Santos et al., 2006) indicate a small influence of  $\epsilon$ -particles on  $\text{H}_2\text{O}_2$  reduction currents at less negative potentials (lower cathodic overpotentials). Thus, a possibility for the enhanced influence of  $\text{HCO}_3^-/\text{CO}_3^{2-}$  in this potential range is that the formation of  $\bullet\text{OH}$  leading to  $\bullet\text{CO}_3^-$  formation is accelerated on these particles. This could then either lead to reformation of  $\text{H}_2\text{O}_2$  (reaction 12) or to its decomposition (reactions 8 and 9). As chemical processes, these reactions would not generate electrochemical current but would reduce the fraction of  $\text{H}_2\text{O}_2$  undergoing current-generating electrochemical reduction. The decomposition of  $\text{H}_2\text{O}_2$  on noble metals is well characterized (McKee, 1969; Serra-Maia et al., 2018).

Presently this suite of reactions cannot be separated, leaving it possible that the overall process is a complex mix of them all.

## 5 Summary

The kinetics of  $\text{H}_2\text{O}_2$  reduction have been studied on  $\text{RE}^{\text{III}}$ -doped  $\text{UO}_2$  specimens and a SIMFUEL, more lightly  $\text{RE}^{\text{III}}$ -doped but also containing noble metal particles. Reduction was shown to proceed *via* the chemical formation followed by electrochemical reduction of  $\text{U}^{\text{V}}$  sites in the  $\text{UO}_2$  surface, with the rate dependent on the availability of  $\text{O}_V$  in the  $\text{UO}_2$  matrix. This availability was significantly greater for the SIMFUEL, leading to more rapid  $\text{H}_2\text{O}_2$  reduction. Also, on the SIMFUEL, the reduction may be slightly enhanced on the noble metal particles.

In the presence of  $\text{HCO}_3^-/\text{CO}_3^{2-}$ , the process is complicated, possibly by the anions ability to cause  $\text{H}_2\text{O}_2$  decomposition and to react with  $\bullet\text{OH}$  radicals, formed by  $\text{H}_2\text{O}_2$  on the surface to yield  $\bullet\text{CO}_3^-$ . These radicals appear to catalyze the reformation of  $\text{H}_2\text{O}_2$  thereby reducing the extent of its electrochemical reduction.

## References

- Badley, M., and Shoesmith, D. (2022). *The corrosion/dissolution of used nuclear fuel in a deep geological repository*. Toronto: Nuclear Waste Management Organization. NWMO-TR-2022-09.
- Bard, A. J., and Faulkner, L. R. (2000). *Electrochemical methods fundamentals and applications*. Second ed. New York: John Wiley & Sons, 819.
- Barreiro Fidalgo, A., Kumagai, Y., and Jonsson, M. (2018). The role of surface-bound hydroxyl radicals in the reaction between  $\text{H}_2\text{O}_2$  and  $\text{UO}_2$ . *J. Coord. Chem.* 71 (11-13), 1799–1807. doi:10.1080/00958972.2018.1466287

## Data availability statement

The raw data supporting the conclusions of this article will be made available by the authors, without undue reservation.

## Author contributions

ZZ: Methodology, Validation, Formal analysis, Investigation, Data curation, Writing—original draft, Visualization. ML: Methodology, data curation, Visualization. NL: Methodology, Supervision. JN: Methodology, Resources, Writing—review and editing, Supervision, Project administration, Funding acquisition. DS: Conceptualization, Methodology, Resources, Writing—review and editing, Supervision, Project administration, Funding acquisition.

## Funding

This research was funded under the Industrial Research Chair and Collaborative Research and Development (CRDPJ 507465–16) agreements between the Natural Sciences and Engineering Research Council (NSERC, Ottawa) and the Nuclear Waste Management Organization (NWMO, Toronto).

## Conflict of interest

The authors declare that the research was conducted in the absence of any commercial or financial relationships that could be construed as a potential conflict of interest.

## Publisher's note

All claims expressed in this article are solely those of the authors and do not necessarily represent those of their affiliated organizations, or those of the publisher, the editors and the reviewers. Any product that may be evaluated in this article, or claim that may be made by its manufacturer, is not guaranteed or endorsed by the publisher.

- Britz, D., and Brocke, W. A. (1975). Elimination of iR-drop in electrochemical cells by the use of a current-interruption potentiostat. *J. Electroanal. Chem. Interfacial Electrochem.* 58 (2), 301–311. doi:10.1016/s0022-0728(75)80088-x
- Ceré, S., Vazquez, M., de Sánchez, S. R., and Schiffrin, D. J. (1999). Surface redox catalysis and reduction kinetics of hydrogen peroxide on copper–nickel alloys. *J. Electroanal. Chem.* 470 (1), 31–38. doi:10.1016/s0022-0728(99)00207-7
- Eriksen, T. E., Shoesmith, D. W., and Jonsson, M. (2012). Radiation induced dissolution of  $\text{UO}_2$  based nuclear fuel – a critical review of predictive modelling approaches. *J. Nucl. Mater.* 420 (1-3), 409–423. doi:10.1016/j.jnucmat.2011.10.027

- Goldik, J. S., Nesbitt, H. W., Noël, J. J., and Shoesmith, D. W. (2004). Surface electrochemistry of  $\text{UO}_2$  in dilute alkaline hydrogen peroxide solutions. *Electrochimica Acta* 49 (11), 1699–1709. doi:10.1016/j.electacta.2003.11.029
- Goldik, J. S., Noël, J. J., and Shoesmith, D. W. (2006b). Surface electrochemistry of  $\text{UO}_2$  in dilute alkaline hydrogen peroxide solutions. *Electrochimica Acta* 51 (16), 3278–3286. doi:10.1016/j.electacta.2005.09.019
- Goldik, J. S., Noel, J. J., and Shoesmith, D. W. (2006a). The effects of simulated fission products in the reduction of hydrogen peroxide on simulated nuclear fuel electrodes. *J. Electrochem. Soc.* 153 (9), E151–E159. doi:10.1149/1.2213419
- Goldik, J. S., Noël, J. J., and Shoesmith, D. W. (2005). The electrochemical reduction of hydrogen peroxide on uranium dioxide electrodes in alkaline solution. *J. Electroanal. Chem.* 582 (1), 241–248. doi:10.1016/j.jelechem.2004.11.007
- Grenthe, I., Fuger, J., Konings, R. J., Lemire, R. J., Muller, A. B., Nguyen-Trung, C., et al. (1992). *Chemical thermodynamics of uranium*, 1. Amsterdam: North-Holland.
- Grenthe, I., and Gaona, X. (2020). *Second update on the chemical thermodynamics of uranium, neptunium, plutonium, americium and technetium*. Paris, France: OECD/NEA Publishing. Report No. NEA-7500.
- Hall, D. S., Behazin, M., Jeffrey Binns, W., and Keech, P. G. (2021). An evaluation of corrosion processes affecting copper-coated nuclear waste containers in a deep geological repository. *Prog. Mater. Sci.* 118, 100766. doi:10.1016/j.pmatsci.2020.100766
- Hall, D. S., and Keech, P. G. (2017). An overview of the Canadian corrosion program for the long-term management of nuclear waste. *Corros. Eng. Sci. Technol.* 52 (1), 2–5. doi:10.1080/1478422x.2016.1275419
- Haygarth, K. S., Marin, T. W., Janik, I., Kanjana, K., Stanisky, C. M., and Bartels, D. M. (2010). Carbonate radical formation in radiolysis of sodium carbonate and bicarbonate solutions up to 250 °C and the mechanism of its second order decay. *J. Phys. Chem. A* 114 (5), 2142–2150. doi:10.1021/jp9105162
- He, H., Broczkowski, M., O'Neil, K., Ofori, D., Semenikhin, O., and Shoesmith, D. (2012). *Corrosion of nuclear fuel ( $\text{UO}_2$ ) inside a failed nuclear waste container*. Toronto, Ontario: Nuclear Waste Management Organization.
- He, H., Keech, P. G., Broczkowski, M. E., Noël, J. J., and Shoesmith, D. W. (2007). Characterization of the influence of fission product doping on the anodic reactivity of uranium dioxide. *Can. J. Chem.* 85 (10), 702–713. doi:10.1139/v07-056
- He, H., and Shoesmith, D. (2010). Raman spectroscopic studies of defect structures and phase transition in hyper-stoichiometric  $\text{UO}_{2+x}$ . *Phys. Chem. Chem. Phys.* 12 (28), 8108–8117. doi:10.1039/b925495a
- Hocking, W., Betteridge, J. S., and Shoesmith, D. W. (1991). *The cathodic reduction of oxygen on uranium dioxide in dilute alkaline aqueous solution*. Canada: Atomic Energy of Canada Limited Report, 1572–6657.
- Hocking, W. H., Betteridge, J. S., and Shoesmith, D. W. (1994). The cathodic reduction of oxygen on uranium dioxide in dilute alkaline aqueous solution. *J. Electroanal. Chem.* 379 (1), 339–351. doi:10.1016/0022-0728(94)87156-6
- Ilton, E. S., Boily, J.-F., and Bagus, P. S. (2007). Beam induced reduction of U(VI) during X-ray photoelectron spectroscopy: The utility of the U4f satellite structure for identifying uranium oxidation states in mixed valence uranium oxides. *Surf. Sci.* 601 (4), 908–916. doi:10.1016/j.susc.2006.11.067
- Keech, P. G., Goldik, J. S., Qin, Z., and Shoesmith, D. W. (2011). The anodic dissolution of SIMFUEL ( $\text{UO}_2$ ) in slightly alkaline sodium carbonate/bicarbonate solutions. *Electrochimica Acta* 56 (23), 7923–7930. doi:10.1016/j.electacta.2010.12.024
- Kwong, G. (2011). *Status of corrosion studies for copper used fuel containers under low salinity conditions*. Toronto, ON: Nuclear Waste Management Organization. Report NWMO TR-2011-14.
- Lide, D. R. (2005). *CRC handbook of chemistry and physics*. Boca Raton, FL: CRC Press, 6–186.
- Liu, N., He, H., Noël, J. J., and Shoesmith, D. W. (2017a). The electrochemical study of  $\text{Dy}_2\text{O}_3$  doped  $\text{UO}_2$  in slightly alkaline sodium carbonate/bicarbonate and phosphate solutions. *Electrochimica Acta* 235, 654–663. doi:10.1016/j.electacta.2017.03.075
- Liu, N., Kim, J., Lee, J., Youn, Y.-S., Kim, J.-G., Kim, J.-Y., et al. (2017b). Influence of Gd doping on the structure and electrochemical behavior of  $\text{UO}_2$ . *Electrochimica Acta* 247, 496–504. doi:10.1016/j.electacta.2017.07.006
- Liu, N., Zhu, Z., Noël, J. J., and Shoesmith, D. W. (2018). “Corrosion of nuclear fuel inside a failed waste container.” In *Encyclopedia of interfacial chemistry: Surface science and electrochemistry* (Amsterdam: Elsevier), Vol. 6, 172–182.
- Lousada, C. M., Trummer, M., and Jonsson, M. (2013). Reactivity of  $\text{H}_2\text{O}_2$  towards different  $\text{UO}_2$ -based materials: The relative impact of radiolysis products revisited. *J. Nucl. Mater.* 434 (1–3), 434–439. doi:10.1016/j.jnucmat.2011.06.003
- Maier, A. C., Kegler, P., Klinkenberg, M., Baena, A., Finkeldei, S., Brandt, F., et al. (2020). On the change in  $\text{UO}_2$  redox reactivity as a function of  $\text{H}_2\text{O}_2$  exposure. *Dalton Trans.* 49 (4), 1241–1248. doi:10.1039/c9dt04395k
- McKee, D. (1969). Catalytic decomposition of hydrogen peroxide by metals and alloys of the platinum group. *J. Catal.* 14 (4), 355–364. doi:10.1016/0021-9517(69)90326-1
- Mühr-Ebert, E. L., Wagner, F., and Walther, C. (2019). Speciation of uranium: Compilation of a thermodynamic database and its experimental evaluation using different analytical techniques. *Appl. Geochem.* 100, 213–222. doi:10.1016/j.apgeochem.2018.10.006
- Nicol, M. J., and Needes, C. R. S. (1973). *The mechanism of the anodic dissolution of uranium dioxide*. Johannesburg, South Africa: National Institute for Metallurgy Report No. 7079.
- Nilsson, S., and Jonsson, M. (2011).  $\text{H}_2\text{O}_2$  and radiation induced dissolution of  $\text{UO}_2$  and SIMFUEL pellets. *J. Nucl. Mater.* 410 (1–3), 89–93. doi:10.1016/j.jnucmat.2011.01.020
- Ofori, D. (2008). *The influence of corrosion product deposits on  $\text{UO}_2$* . London, ON: University of Western Ontario.
- Razdan, M., Hall, D. S., Keech, P. G., and Shoesmith, D. W. (2012). Electrochemical reduction of hydrogen peroxide on SIMFUEL ( $\text{UO}_2$ ) in acidic pH conditions. *Electrochimica Acta* 83, 410–419. doi:10.1016/j.electacta.2012.05.163
- Razdan, M., and Shoesmith, D. W. (2014). Influence of trivalent-dopants on the structural and electrochemical properties of uranium dioxide ( $\text{UO}_2$ ). *J. Electrochem. Soc.* 161 (3), H105–H113. doi:10.1149/2.047403jes
- Razdan, M., Trummer, M., Zagidulin, D., Jonsson, M., and Shoesmith, D. W. (2014). Electrochemical and surface characterization of uranium dioxide containing rare-earth oxide ( $\text{Y}_2\text{O}_3$ ) and metal (Pd) particles. *Electrochimica Acta* 130, 29–39. doi:10.1016/j.electacta.2014.02.134
- Regino, C. A. S., and Richardson, D. E. (2007). Bicarbonate-catalyzed hydrogen peroxide oxidation of cysteine and related thiols. *Inorganica Chim. Acta* 360 (14), 3971–3977. doi:10.1016/j.ica.2007.05.020
- Richardson, D. E., Yao, H., Frank, K. M., and Bennett, D. A. (2000). Equilibria, kinetics, and mechanism in the bicarbonate activation of hydrogen peroxide: Oxidation of sulfides by peroxydicarbonate. *J. Am. Chem. Soc.* 122 (8), 1729–1739. doi:10.1021/ja9927467
- Santos, B. G., Nesbitt, H. W., Noël, J. J., and Shoesmith, D. W. (2004). X-ray photoelectron spectroscopy study of anodically oxidized SIMFUEL surfaces. *Electrochimica Acta* 49 (11), 1863–1873. doi:10.1016/j.electacta.2003.12.016
- Santos, B. G., Noël, J. J., and Shoesmith, D. W. (2006). The effect of pH on the anodic dissolution of SIMFUEL ( $\text{UO}_2$ ). *J. Electroanal. Chem.* 586 (1), 1–11. doi:10.1016/j.jelechem.2005.09.021
- Schindler, M., Hawthorne, F. C., Freund, M. S., and Burns, P. C. (2009). XPS spectra of uranyl minerals and synthetic uranyl compounds. I: The U 4f spectrum. *Geochimica Cosmochimica Acta* 73 (9), 2471–2487. doi:10.1016/j.gca.2008.10.042
- Serra-Maia, R., Bellier, M., Chastka, S., Tranhuu, K., Subowo, A., Rimstidt, J. D., et al. (2018). Mechanism and kinetics of hydrogen peroxide decomposition on platinum nanocatalysts. *ACS Appl. Mat. Interfaces* 10 (25), 21224–21234. doi:10.1021/acsami.8b02345
- Sunder, S., Miller, N. H., and Shoesmith, D. W. (2004). Corrosion of uranium dioxide in hydrogen peroxide solutions. *Corros. Sci.* 46 (5), 1095–1111. doi:10.1016/j.corsci.2003.09.005
- Trunov, A., and Presnov, V. (1975a). Oxygen electroreduction on semiconductor catalysis II: Processes at oxide semiconductor-electrolyte interface. *Elektrokhimiya* 11 (1), 77–84.
- Trunov, A., and Presnov, V. (1975b). Oxygen electroreduction on semiconductor catalysis III: The importance of 3d electrodes of oxide semiconductor. *Elektrokhimiya* 11 (1), 290–292.
- Vazquez, M. V., de Sanchez, S. R., Calvo, E. J., and Schiffrin, D. J. (1994). The electrochemical reduction of hydrogen peroxide on polycrystalline copper in borax buffer. *J. Electroanal. Chem.* 374 (1), 179–187. doi:10.1016/0022-0728(94)03342-0
- Wu, L., and Shoesmith, D. W. (2014). An electrochemical study of  $\text{H}_2\text{O}_2$  oxidation and decomposition on simulated nuclear fuel (SIMFUEL). *Electrochimica Acta* 137, 83–90. doi:10.1016/j.electacta.2014.06.002
- Zhu, Z., Noël, J. J., and Shoesmith, D. W. (2020). Hydrogen peroxide decomposition on simulated nuclear fuel bicarbonate/carbonate solutions. *Electrochimica Acta* 340, 135980. doi:10.1016/j.electacta.2020.135980
- Zhu, Z., Wu, L., Noël, J. J., and Shoesmith, D. W. (2019). Anodic reactions occurring on simulated spent nuclear fuel (SIMFUEL) in hydrogen peroxide solutions containing bicarbonate/carbonate – the effect of fission products. *Electrochimica Acta* 320, 134546. doi:10.1016/j.electacta.2019.07.057